Measurement of the dijet cross section in 400-GeV/c pp interactions

M. W. Arenton,[a,*] H. F. Chen,[g,†] M. Corcoran,[f] L. Cormell,[e,*] W. R. Ditzler,[a] M. Dris,[e,‡] A. R. Erwin,[g] T. Fields,[a] J. Fleischman,[e] E. Gardella,[e] R. Gustafson,[d] M. Harrison,[b] M. A. Hasan,[g] C. Hitzman,[e,§] K. Johns,[f] A. Kanofsky,[c] W. Kononenko,[e] C. E. Kuehn,[g] H. E. Miettinen,[f] C. Naudet,[f] K. S. Nelson,[g] J. Rice,[f,**] J. Roberts,[f] B. Robinson,[e] W. Selove,[e] G. Theodosiou,[e] M. A. Thompson,[g] and B. Yost[e,††]

[a]*Argonne National Laboratory, Argonne, Illinois 60439*
[b]*Fermilab, Batavia, Illinois 60510*
[c]*Lehigh University, Bethlehem, Pennsylvania 18015*
[d]*University of Michigan, Ann Arbor, Michigan 48109*
[e]*University of Pennsylvania, Philadelphia, Pennsylvania 19104*
[f]*Rice University, Houston, Texas 77001*
[g]*University of Wisconsin, Madison, Wisconsin 53706*

(Received 9 April 1984)

The invariant cross section for production of jet pairs in 400-GeV/c pp interactions has been measured as a function of p_T in the p_T range 4 to 9 GeV/c. The results are in good agreement with predictions of a perturbative QCD model. Details of the experiment and the procedures used to extract the jet signal are given.

I. INTRODUCTION

The study of jet production in hadronic interactions has been motivated by the expectation that the jets directly reflect the underlying parton-parton scattering. Early studies of high-p_T single particles have provided results that, while giving information on the nature of the hard scattering process, do not directly measure the parton scattering cross section.[1] Recently, however, clear evidence for jet production in hadronic interactions has been observed. This evidence is visually striking at the 540-GeV center-of-mass energy of the CERN SPS collider,[2,3] and is also clear at the highest CERN ISR energies.[4] At the lower energies of Fermilab and SPS fixed-target experiments the situation is more complicated.[5,6] Nevertheless, as we have shown in previous papers,[7] jets can definitely be seen at these lower energies. Here we extend and refine our analysis in order to determine the invariant cross section for the production of jet pairs.

This article is organized as follows. First the experimental apparatus and its calibration are described. Then we proceed to discuss the analysis, the main parts of which are the methods for determining the jet signal and the calculations of the trigger efficiency. We then present the results on the dijet cross section and compare them with predictions of a simple theoretical model. More detailed discussions of resolution questions and of procedures for estimating the background are given in the Appendices.

II. EXPERIMENTAL METHOD

A plan view of experiment E-609, located in the M6 beam line at Fermilab, is shown in Fig. 1. The 400-GeV/c proton beam was incident on a 45-cm liquid hydrogen target. Since rare processes such as high-p_T jet production may be faked by (or even obscured by) accidental coincidences of more common events, special precautions were taken to ensure that only a single beam particle entered the target. A dE/dx counter in the beam rejected cases with more than one beam particle in the same rf bucket. Pile-up circuitry rejected beam particles with a second beam particle within ± 110 ns, the width of the analog-to-digital-converter (ADC) gates. A wall of veto counters embedded in the massive iron shield upstream of the apparatus rejected events accompanied by muons. The average beam flux eligible to make events after these requirements was 1.5×10^5 per 1-s spill. The total integrated luminosity used in the results reported here was 7.5×10^{33} cm^{-2}.

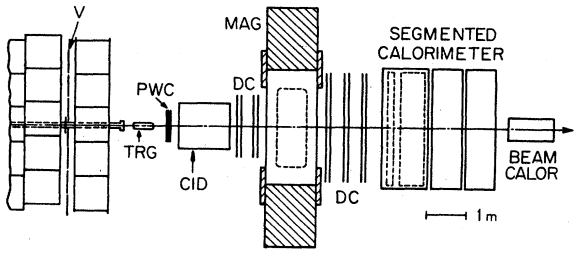

FIG. 1. Plan view of the E-609 experiment. V, veto counters; TRG, hydrogen target; DC, drift chambers.

Following the target was a magnetic spectrometer consisting of a 1×3-m aperture analyzing magnet surrounded by planes of proportional and drift chambers. The magnet was operated with a low transverse-momentum kick of 100 MeV/c to avoid complicating the geometrical triggers (described below) which assumed straight-line trajectories. In the present analysis the charged-particle tracking has been used only to determine the position of the production vertex to separate events occurring in the target hydrogen from background events produced else-

where.

Included in the upstream part of the spectrometer for part of the data taking was a ring-imaging Cherenkov counter designed to identify particles in the high-p_T jets.

The heart of the apparatus is the large segmented calorimeter. The calorimeter was divided transversely into 132 towers, which approximately pointed back to the target. The arrangement of the towers is shown in Fig. 2, which also shows the center-of-mass polar angles for the 400-GeV/c beam. Each tower is composed of one lead-scintillator module and three iron-scintillator modules, each with its own phototube.[8] The calorimeter modules vary in thickness and proportion of absorber to scintillator with the polar angle from the beam, since more absorber is needed to contain the energetic particles near the beam while finer sampling is needed to obtain good energy resolution for the lower-energy particles at large angles. The lead layer varied in thickness from 8.8 to 5.4 radiation lengths. The iron layers varied from 7.6 to 5.8 absorption lengths.

Signals from the four layers were summed in the analysis with weighting to obtain the best resolution for both hadrons and photons from π^0 decay. The last two layers were weighted at 1.25 times the front two layers to compensate for the fact that the mean energy deposited by a hadron is only about 75% of that for a photon.

Each of the 528 calorimeter modules was equalized in pulse-height response by steering a beam of muons through it and adjusting the phototube high voltage to give the proper pulse height. The momentum calibration of the calorimeter was then determined by steering beams of hadrons and electrons of various energies into several places in the calorimeter. In this way the energy resolution was determined to be typically $70\%/\sqrt{E}$ for hadrons and $35\%/\sqrt{E}$ for electrons (E in GeV).

In the final analysis, an unfolding of the energy resolution from the distribution in transverse momentum observed in the data must be performed to yield the correct p_T distribution. This unfolding can be achieved by multiplying the observed energy by a factor whose value depends on the steepness of the p_T distribution and the energy resolution of the calorimeter.[9] (It also depends on the relative fraction of electromagnetically and hadronically interacting particles in the jet.) This factor was calculated by Monte Carlo techniques. The value used, appropriate for the observed dN/dp_T for dijets of $\exp(-1.6p_T)$, was 0.99. This value arises as follows. We defined the pulse-height/energy ratio to be 1.00 for electromagnetic energy. Hadronic energy produces a pulse-height/energy ratio of about 0.75. Thus a flat p_T distribution consisting of one-third electromagnetic energy and two-thirds hadronic energy would require a factor to convert pulse height to energy of $1/(\frac{1}{3}+\frac{2}{3}\times 0.75)$ or about 1.2. Actually it is somewhat smaller than this because we have partially corrected for the difference between hadronic and electromagnetic energy by multiplying the two downstream calorimeter layer energies by 1.25. If half the hadronic energy goes into these two layers the factor for a flat p_T distribution would be 1.12. The rapidly falling p_T distribution compensates rather closely for this needed factor, producing the final factor of 0.99. This resolution effect is discussed further in Appendix A.

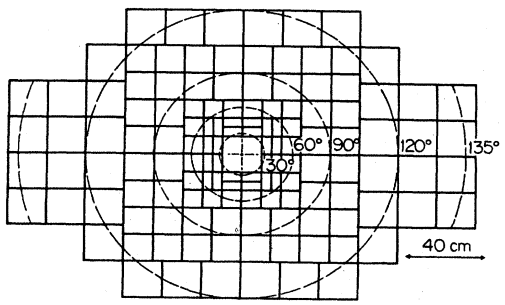

FIG. 2. Cross section of the front face of the calorimeter showing the transverse segmentation of the array. The circles show center-of-mass polar angles for 400-GeV/c pp interactions.

The apparatus also included a downstream calorimeter covering the beam hole in the main calorimeter to measure the energy in the event that went close to the beam direction.

Triggers for the experiment required a good beam particle in coincidence with some requirement on the transverse-energy deposition in the calorimeter. Transverse-energy E_T is taken as the energy detected in a calorimeter tower times the sine of its polar angle. Most triggers required that the sum of E_T observed in some group of calorimeter towers exceed a threshold.[10] Various such groups were used concurrently, ranging from the entire calorimeter (the so-called global trigger) to various sized groups of towers on opposite sides of the calorimeter (the so-called double-arm triggers).

The results presented here, however, used a somewhat different trigger, which we call the two-high trigger. This required that any two calorimeter towers each have more than a certain threshold in E_T. The threshold was chosen high enough ($p_T \sim 1.2$ GeV/c) to be selective for jetlike events, but not so high as to select only events where the jet fragmented primarily into a single high-p_T particle. This trigger is geometrically unbiased, uses the whole calorimeter, and has a high detection efficiency for jet events.

We are also analyzing the double-arm trigger data to obtain the dijet cross section and will present the results of that analysis in a separate publication.

While the two-high trigger is not subject to such a specific geometrical bias as is a double-arm trigger, it of course has its own set of biases that must be corrected for in the analysis. Since the two-high requirement involves individual calorimeter towers, it is biased toward events where a large fraction of a particle's energy appears in a single tower. In particular, this means that there is a bias toward jets that fragment into a leading π^0, since electromagnetic energy is contained within smaller transverse dimensions in the calorimeter than is hadronic energy. There are also some (fairly small) differences of the center-of-mass solid angle of the various towers, which leads to some variation of trigger efficiency with c.m. an-

gle. All such systematic trigger biases are fully taken into account in the Monte Carlo calculation of the trigger efficiency, which is described in detail in Sec. III E. Additionally, it should be pointed out that any method of isolating jet events in hadron collisions, even at the highest energies, requires an evaluation of the effects of "trigger bias" which inevitably results from whatever on-line and off-line selection criteria are used.

III. THE ANALYSIS

There are two main steps in determining the dijet cross section from the two-high-trigger data. The first is finding how many jet events in each p_T interval are in the data. The second is calculating the efficiency with which such jets satisfy the trigger.

A. Preliminaries

Some preliminaries were done first. The ADC readings of the energies in the calorimeter modules were corrected for ADC nonlinearities and converted to energies. The trigger was then reapplied in software in order to select a sharp threshold. Figure 3 shows the distributions of the highest-p_T and second-highest-p_T calorimeter tower in the events before software cuts. We chose software cuts of 1.57 GeV/c on the highest-p_T tower and 1.38 GeV/c on the second-highest-p_T tower.

Subsequent analysis requires knowledge of the momenta of the particles that hit the calorimeter rather than just the energies deposited in the various towers. An algorithm was used to reconstruct particle momenta from the pattern of energy deposition in the calorimeter towers. This algorithm was based on the properties of showers measured in the calibration data using hadron and electron beams.

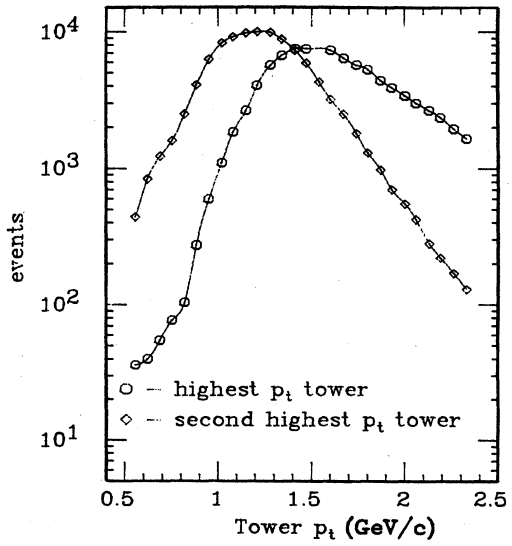

FIG. 3. Distributions in p_T of the highest- and second-highest-p_T calorimeter tower in two-high-trigger events. Software cuts were applied at the points where the curves begin to decrease exponentially.

B. The Monte Carlo program

Several aspects of the analysis make use of a Monte Carlo program, which we describe here. A brief description of this program has been published,[11] and a detailed article concerning it, which includes many comparisons with data from this and other experiments, is in preparation.[12]

The Monte Carlo is a "four-jet" model that generates two scattered jets according to first-order QCD cross sections, as well as a beam and a target jet. The jets are fragmented to hadrons according to the prescription of Field and Feynman.[13] Both the momentum transfer squared in the parton-parton scattering $\hat{t}$ as well as $\hat{u}$ are allowed to be as small as 1 GeV.[2] This model does reasonably well in representing several key features of real data, most notably the nonjetlike appearance (low planarity) of most global trigger events. This is seen in Fig. 4(a), which shows

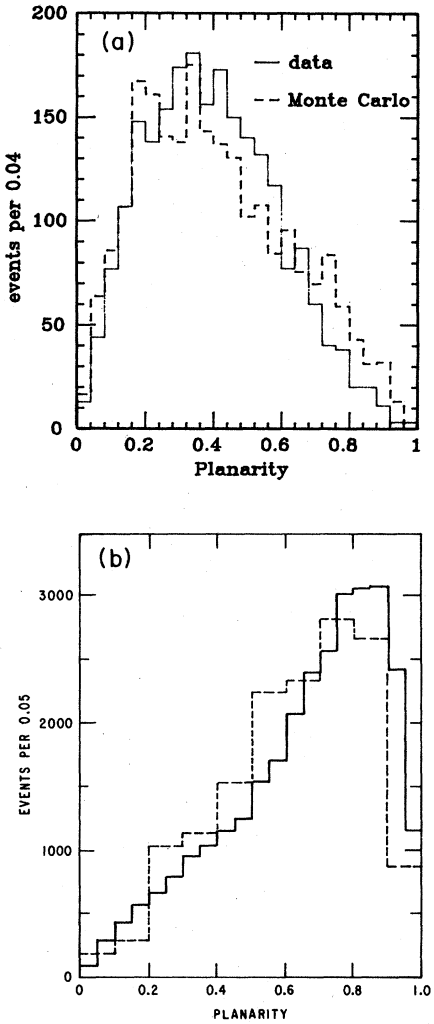

FIG. 4. (a) Comparison of the planarity distributions of global-trigger events with $E_T > 11$ GeV from this experiment with the distribution predicted by the Monte Carlo program. (b) Same comparison for two-high-triggered events.

the planarity distributions of global E_T trigger data with an E_T threshold of 11 GeV compared to the prediction of the Monte Carlo. Figure 4(b) shows that the Monte Carlo prediction for the planarity distribution of the two-high triggered events is also quite similar to the experimental data.

Note that every event in this model has jets, and the "background" for high-p_T jets arises from the combination of particles from jets of lower p_T with particles originating in the beam and target jets.

The program samples the rapidly falling cross section in p_T by generating events with a relatively flat $\hat{t}$ distribution and weighting the events by the QCD cross section.

Energies in each calorimeter module were generated from the Monte Carlo particles by simulating the energy resolution and shower spreading. Charged-particle trajectories were bent by the spectrometer magnet in the simulation, although this is a very small effect. Each π^0 decayed into two photons and the photons were treated separately in the ensuing simulation. The measured resolutions, different for the various types of calorimeter towers, for hadrons and electrons were used to smear the particle energies. The transverse spreading of hadronic showers (as well as that for electromagnetic showers) was parametrized as the sum of two two-dimensional Gaussians. The energies in individual modules calculated from the transverse spreading were further randomized by 10% to take into account fluctuations in the spreading. The longitudinal distribution of shower energy was based on the parametrization of Bock *et al.*[14]

C. Jet finding

Of all the events satisfying the trigger, one next has to find the relatively small fraction which are high-p_T jet events. A jet-finding algorithm was used for this task. Basically the algorithm attempts to find all particles within a cone of half-angle α about a jet axis. Working with the particle momenta in the pp center-of-mass system (all particles are assumed to be pions when transforming to the c.m.), the algorithm first finds the particle with the highest p_T. If this particle's p_T is greater than some cutoff (we have used 0.5 GeV/c), its momentum vector is used as the initial estimate of the jet axis. The algorithm then searches for any particles within an $\alpha/5$ half-angle cone about this axis. Any particles found have their momenta vectorially added to the axis to define a new axis. The search is then made in a $2\alpha/5$ cone around the new axis.

This continues for five steps until the angle α is reached. During this search, particles within a certain angle of the beam direction (30°) are not allowed to be added to the jet. Since the calorimeter coverage begins at about 30° this has little effect. The particles found for this jet are then excluded from consideration and the algorithm starts again to search for another jet. After no suitable starting particles remain, the algorithm examines all pairwise combinations of the found jets and if the relative p_T of the two is less than a cutoff (1 GeV/c) combines then into a single jet. Finally, the algorithm examines every particle in each jet and calculates whether it is closer in angle to the axis of some other jet, and if so that particle is moved to the other jet.

Note that this algorithm is not restricted as to the number of jets it can find in an event. For the subsequent analysis, we have taken for the jet p_T of the event the average p_T of the two highest-p_T jets in the event. Typically in our data sample about $\frac{2}{3}$ of the events with jet p_T greater than 3 GeV/c have two jets found and the other $\frac{1}{3}$ have three jets found. No restriction is placed on the c.m. angles of the two jets by the jet-finding algorithm, and in particular they are not required to be coplanar. Applying the algorithm to Monte Carlo events we find that it correctly finds the angles of the jets with standard deviations of about 5° in both the azimuthal and polar angle. Thus we define a dijet event to be one where the jet-finding algorithm finds at least two jets, and take its p_T to be the average of the two highest-p_T jets in the event.

Although the jet-finding algorithm does not require it, the high-p_T jets found in the data do indeed have the properties one would expect of jets; namely, the two high-p_T jets are 180 degrees apart in azimuth and roughly balance p_T. This is shown in Figs. 5 and 6 which show, for events with jet p_T greater than 4 GeV/c, the difference in azimuth between the two jets and the absolute value of the difference in p_T, respectively. Note that only 3059 events with jet p_T greater than 4 GeV/c, including 187 of jet $p_T > 6$ GeV/c, were found out of a sample of 30 281 events passing the two-high software threshold.

The cone half-angle α is of course a most important parameter in determining the exact value of jet p_T found. The optimum value of α was found from the Monte Carlo model. To avoid background events that really do not have high-p_T jets, only events with jets of p_T greater than 3 GeV/c were used for this study. The two-high trigger

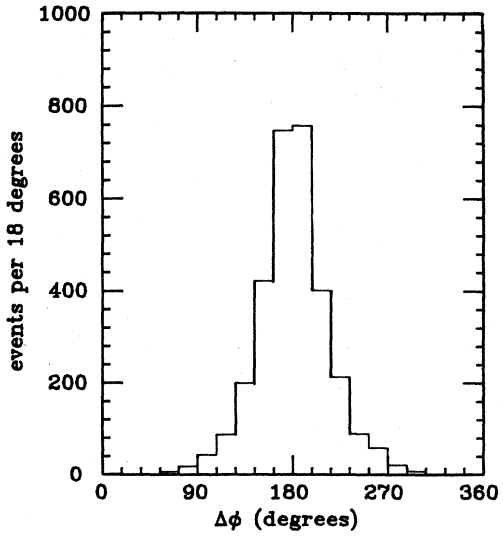

FIG. 5. The difference in azimuthal angle between the two highest-p_T jets found in the data for events with jet p_T greater than 4 GeV/c.

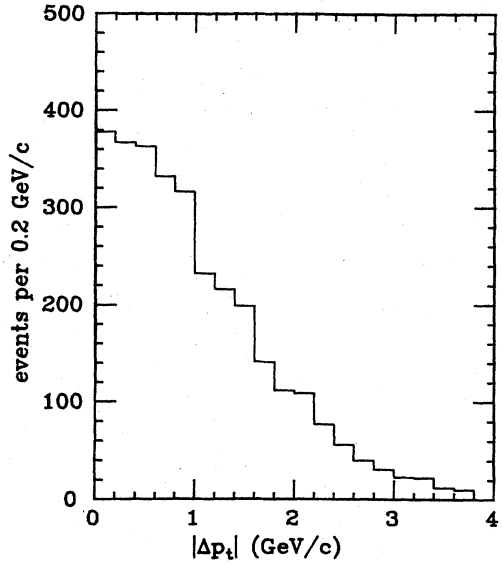

FIG. 6. The absolute value of the difference in p_T between the two highest-p_T jets found in the data for events with jet p_T greater than 4 GeV/c.

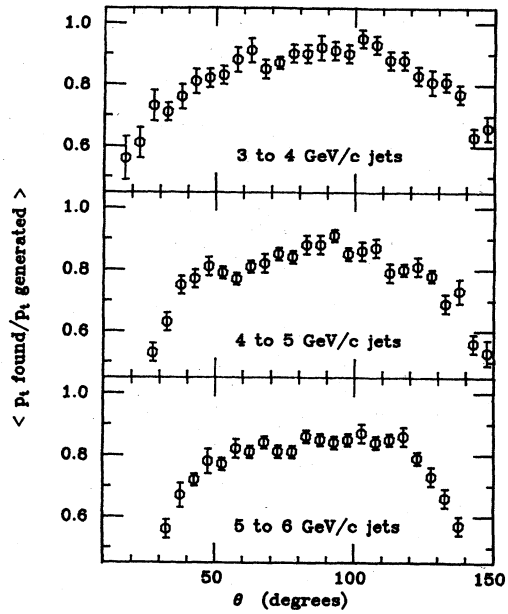

FIG. 7. The average value of the ratio of p_T found by the jet-finding algorithm to the generated p_T versus the polar angle of the jet for three ranges of jet p_T, calculated using the Monte Carlo program. A flat p_T distribution was used.

was imposed on the Monte Carlo model events, and then the same analysis as for real data was performed on the events passing the trigger. The results for the number of events found versus p_T are compared with the original event sample passing the trigger cuts in Table I, for various choices of the cone angle α in the jet-finding algorithm. The best agreement between the original Monte Carlo and the events found by the analysis is for $\alpha=55°$. A 5° change in α changes the invariant cross section determined at 6-GeV/c jet p_T by about 30%.

The determination of cross sections must be restricted to a fiducial region in the calorimeter, since jets striking near the calorimeter edges will not have all of their energy measured. Figure 7 shows the average value of the p_T found by the jet-finding algorithm using Monte Carlo events including full simulation of the calorimeter resolution as a function of the polar angle of the jet. The results are shown for several ranges of jet p_T. The curves do not plateau at 1.0 because they use a flat distribution in jet p_T. The difference from 1 corresponds approximately to the equivalent energy-scale-factor effect of the actual steep p_T distribution, as mentioned earlier.

Of course, this calculation does include the effects of loss or gain of p_T from beam and target fragments. Figure 7 includes all events of the indicated p_T range. A calculation only including those events that satisfy the two-high trigger yields similar results. Figure 7 indicates good jet containment in the angular region 60° to 100°. We have used this range as the fiducial region, requiring the axes of both jets to be within it.

D. Estimating the true number of jets

Having found the events that appear to have high-p_T jets (about 20% of the events have jets found above 3 GeV/c), the next question is: what fraction of the events found are actually jets as opposed to some other background process that could simulate jets? Key concepts and procedures for estimating the fraction of true jet events are presented in Appendix B.

TABLE I. Monte Carlo analysis used to determine the optimum-cone half angle in the jet-finding algorithm. The first column gives the number of weighted Monte Carlo events (arbitrary units) passing the trigger cuts versus p_T. The remaining columns give the number of events found by the algorithm for three choices of the cone angle.

Jet p_T (GeV/c)	Generated	Found with cone of 50 degrees	55 degrees	60 degrees
4–5	$(1.3\pm0.1)\times10^{-3}$	$(1.8\pm0.1)\times10^{-3}$	$(1.9\pm0.1)\times10^{-3}$	$(2.0\pm0.1)\times10^{-3}$
5–6	$(9.9\pm1.2)\times10^{-4}$	$(7.8\pm0.5)\times10^{-4}$	$(9.0\pm0.6)\times10^{-4}$	$(1.0\pm0.1)\times10^{-3}$
6–7	$(3.7\pm0.3)\times10^{-4}$	$(3.2\pm1.0)\times10^{-4}$	$(3.4\pm0.4)\times10^{-4}$	$(4.2\pm0.4)\times10^{-4}$
7–8	$(1.3\pm0.1)\times10^{-4}$	$(4.7\pm0.7)\times10^{-5}$	$(1.6\pm1.0)\times10^{-4}$	$(1.9\pm1.0)\times10^{-4}$
8–9	$(1.7\pm0.2)\times10^{-5}$	$(6.5\pm1.4)\times10^{-6}$	$(1.0\pm0.1)\times10^{-5}$	$(1.4\pm0.2)\times10^{-5}$

A simple model-independent method which we will refer to as method I involves the use of a randomizing procedure in which the individual particle momentum vectors are rotated randomly in both polar and azimuthal angle, subject to the constraint that the vector sum of the individual particle p_T vectors remain constant. We call this procedure "scrambling." The method-I procedure, then, is to take a sample of real global trigger events in the E_T range one is interested in, scramble them, impose the trigger requirement, and then find how many jets there appear to be in this sample of randomized events whose particles have the minimum angular correlations which are consistent with momentum conservation. Since one must use the calorimeter simulation to determine if the scrambled event satisfies the trigger, the exact procedure uses much computer time. Also, a very large sample of global trigger events is needed to obtain a statistically significant final sample of randomized events satisfying the trigger.

For these reasons an alternate, slightly approximate, procedure was followed. If one uses a particle two-high trigger, that is, a trigger requiring any two *particles,* rather than the calorimeter-tower two-high trigger, then these events, after scrambling, still satisfy the trigger (and of course they are the only events that could ever satisfy this trigger). So it is fairly easy to do a scrambling analysis for a two-high particle trigger. Of course the background calculated from the particle trigger may not be quite the same as for the two-high tower-p_T trigger.

Such a software particle trigger was imposed on the regular two-high data sample. Particle-p_T thresholds used were 2.2 and 1.9 GeV/c. The second column in Table II shows the ratio of scrambled to data events. The scrambling preserved the net momentum vector to within 0.5 GeV/c. To improve statistics each event was scrambled five times.

Examining these results we see that above 4 or 5 GeV/c an increasing fraction of the events are really jets and not fluctuations. As explained in Appendix B, method I gives only an upper limit on the nonjet fraction, however, and the actual fraction might be much lower (see Appendix B). We have investigated this question, first by applying the scrambling technique to Monte Carlo four-jet events, where by construction there is no nonjet background.

TABLE II. Scrambling analysis of events selected using a two-high particle trigger as described in the text (method I). The ratio of events found after scrambling to the original number is given as a function of p_T. The first column gives the results from the experimental data, and the second the results from Monte Carlo events.

Jet p_T (GeV/c)	Data Scrambled/Original	Monte Carlo Scrambled/Original
3–4	1.17±0.03	0.58±0.21
4–5	1.08±0.03	0.75±0.12
5–6	0.91±0.04	0.40±0.11
6–7	0.54±0.05	0.61±0.14
7–8	0.39±0.08	0.28±0.15
8–9	0.17±0.09	0.17±0.05

The result is shown in the third column of Table II. Comparing with the results for the data we conclude that for $p_T > 5$ GeV/c the nonjet fraction found by method I is consistent with being entirely caused by accidental overlap of lower-energy jets with fragments from beam and target fragmentation. It is clear that such an apparent (but false) nonjet fraction is in fact an intrinsic part of any four-jet model. Consequently, an alternate approach, which we refer to as method II, is to use the Monte Carlo model to directly calibrate the overall efficiency of our jet-finding procedure, including background effects. We have carried out such a study, again using our Monte Carlo sample which includes the entire range of generated jet-p_T values from 1 GeV/c on up.

This calculation was done simply by taking the Monte Carlo event sample, imposing the trigger cuts, and comparing the number of events that were found by the jet-finding algorithm at a given p_T with the number of events that were actually generated at that p_T. The results of method II are shown in Table III. We see that below 6 GeV/c more events were found than were generated. This effect arises in the model from events with very low p_T jets (typically less than 2 GeV/c), which, as a result of being combined with additional particles from the beam and target jets, are found to lie at higher than their true p_T by the jet-finding algorithm. This background effect is discussed in Appendix B.

A completely different method of estimating an upper limit to the nonjet fraction, as mentioned in Appendix B, is to generate events randomly using the same single-particle p_T distributions as for global trigger events in the appropriate E_T range. We call this method III. A calculation of this type was done using the single-particle p_T distribution from a sample of global trigger data with E_T greater than 8 GeV. Events were generated with global E_T's between 8 and 20 GeV, distributed according to the observed global trigger E_T distribution. The azimuthal angle of the particles was generated uniformly and the polar angle according to the experimentally observed distribution. The events were then forced to conserve transverse momentum to the same extent as real data by means of a transverse Lorentz boost in the direction opposite to the event's net transverse-momentum vector. In all 900 000 events were generated, which corresponds to a cross section sensitivity 4.13 times less than the real data from the experiment. We compare these events to the data using the same particle two-high trigger that was used in method I. The calculation only gives results for jet p_T's greater than 4 GeV/c since a global E_T threshold of 8 GeV was used. We find 103 events in the random sample with jet p_T's between 4 and 5 GeV/c and 14 between 5 and 6 GeV/c, with none at higher jet p_T's. Correcting for the difference in sensitivity this gives ratios of random events to real events of 0.27±0.03 for 4 to 5 GeV/c and 0.12±0.03 for 5 to 6 GeV/c. Since in method III we did not simulate the calorimeter response, the exact percentage of events satisfying the trigger is somewhat uncertain. However, in any case method III shows that the background is very small above 6 GeV/c.

Several general conclusions can be drawn from these

TABLE III. The fraction of nonjet background found by the jet-finding analysis for Monte Carlo data passing the two-high trigger (method II).

p_T (GeV/c)	Generated	Found	Fraction background
3–4	$(1.5\pm1)\times10^{-3}$	$(3.1\pm0.4)\times10^{-3}$	0.53±0.07
4–5	$(1.3\pm0.1)\times10^{-3}$	$(2.6\pm0.2)\times10^{-3}$	0.48±0.05
5–6	$(9.9\pm1.2)\times10^{-4}$	$(1.5\pm0.3)\times10^{-3}$	0.34±0.17
6–7	$(3.7\pm0.3)\times10^{-4}$	$(3.5\pm0.4)\times10^{-4}$	0
7–8	$(1.3\pm0.1)\times10^{-4}$	$(1.6\pm1.0)\times10^{-4}$	0
8–9	$(1.7\pm0.2)\times10^{-5}$	$(1.0\pm0.2)\times10^{-5}$	0

various methods of estimating the fraction of nonjet events. First, all three methods agree that the sample above about 6-GeV/c jet p_T is almost entirely real jets, and that between 5 and 6 GeV/c the sample is predominantly jets. At p_T's below about 5 GeV/c, there is certainly a significant fraction of nonjet events in the sample. The bin from 3 to 4 GeV/c has a large uncertainty in its background content. We have in the following analysis assumed that there is no contamination from nonjets above 6 GeV/c and used the nonjet fraction calculated using method II (Table III) to correct the data at lower jet p_T's.

An indication of the consistency of these conclusions can be seen by examining the planarity distributions of the data. Planarity should be near one for jets (the Monte Carlo indicates that it should peak at about 0.8 for high-p_T jets). Figure 8 shows the planarity distributions for the data divided into bins of jet p_T as found by the jet-finding algorithm. There is a peak at high planarity in all bins but at the lower p_T's there also is a broader distribution in planarity as well. This appears consistent with the interpretation that there is a fraction of nonjet events of order 50% below 5 GeV/c.

E. Calculation of the trigger efficiency

Once the number of jet events is determined, the other quantity needed to determine the cross section is the trigger efficiency. This was calculated using the Monte Carlo program.

It is important to check how well the simulation corresponds to the actual data. Figure 9 shows, as a function of jet p_T, the average global E_T in the event. The agreement between data and Monte Carlo is fairly good. This particular comparison checks how well the Monte Carlo reproduces the beam jet contribution to the global E_T, which is important because a certain fraction of the two-

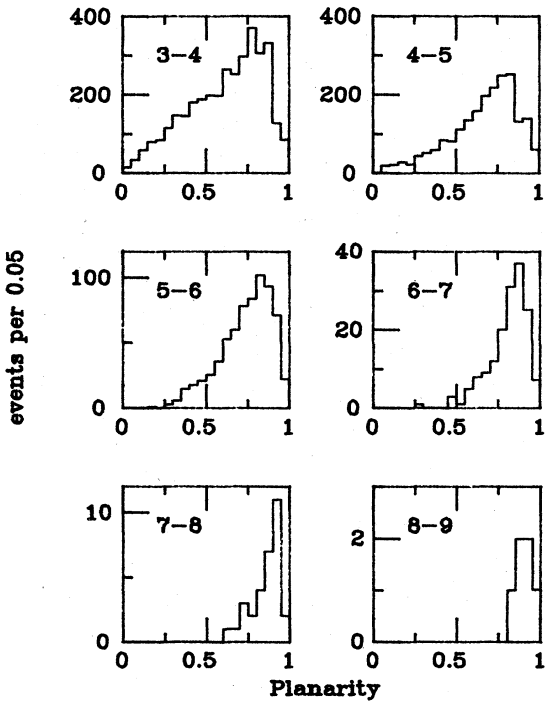

FIG. 8. Planarity distributions of the two-high-trigger data for six bins in jet p_T.

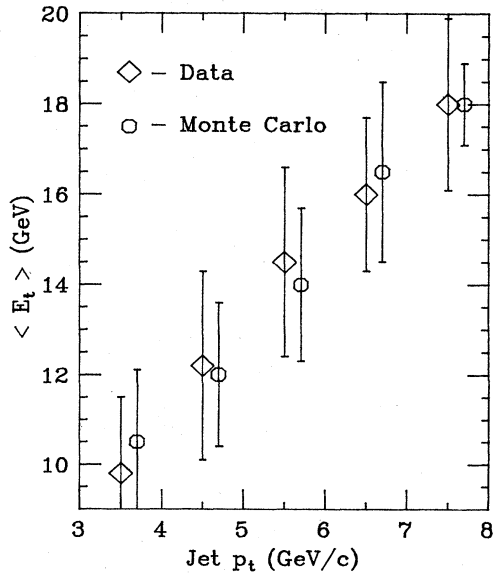

FIG. 9. Comparison of the average total global transverse energy as a function of jet p_T for data and Monte Carlo events. The error bars indicate the rms widths of the transverse-energy distributions.

high triggers, especially at lower jet p_T's, come from beam-jet particles providing one or both of the two-high tower p_T's. Comparisons also have been made of the average particle multiplicity in data and Monte Carlo with the result that $\sim 30\%$ more particles are found in the data, perhaps due to an inadequate treatment of fluctuations in the shower spreading.

The trigger efficiency was calculated simply as the number of Monte Carlo events satisfying the trigger divided by the number generated. The results, along with their statistical errors, are shown in Fig. 10.

Since the trigger efficiency is an important element in the cross-section determination, it is important to estimate the systematic uncertainties involved in its calculation. Two principal sources of error have been considered. The first arises from uncertainties in the transverse spreading of the showers in the calorimeter. Examination of the analysis used to determine the size of the shower spreading (using data where a hadron beam was sent into various places in the calorimeter array), showed that the spreading for electromagnetically interacting particles could be 20% smaller or 25% larger than the nominal values, and for hadronically interacting particles 10% smaller or 25% larger. The trigger efficiencies were recalculated using these limits on shower spreading. The results are shown in Table IV. The major effect is from the hadronic spreading, since most electromagnetic showers fit within a single tower in any case, while the fraction of hadronic shower energy in a single tower is sensitive to the spreading.

Another source of systematic uncertainty that we have examined is the dependence on the physics assumptions made in the Monte Carlo, particularly on the form of the jet fragmentation into hadrons, since a fragmentation yielding a softer or harder particle distribution will change the fraction of particles capable of satisfying the two-high trigger. We have examined this question by calculating the efficiencies using a different Monte Carlo program, ISAJET.[15] An important difference between ISAJET and our Monte Carlo program is that ISAJET incorporates scale breaking in the parton fragmentation, while our program does not. In making the comparison it was found that ISAJET does not simulate the properties of the beam jet in a way consistent with experimental data. In particular the average global E_T for a given jet p_T was much smaller than that seen in the real data. To avoid the effects of this we compared the trigger efficiencies of the two programs using only the particles from the two high-p_T jets. The result is given in Table V.

As expected, ISAJET gives a lower efficiency (which mainly affects lower-p_T values) due to the softer p_T distribution resulting from scale breaking in the fragmentation. Again, our 3-to-4-GeV/c bin is clearly the most uncertain.

IV. THE RESULTS

A. Experimental results

The actual invariant cross section for a given bin in jet p_T is calculated from

$$d\sigma/dp_T{}^2dy_1dy_2 = N_{\text{evts}} \times (\text{nonhydrogen correction}) \times [(\text{beam flux}) \times (\text{target density}) \times (\text{target length}) \times (\text{trigger efficiency}) 2p_T \Delta p_T \Delta y_1 \Delta y_2]^{-1} .$$

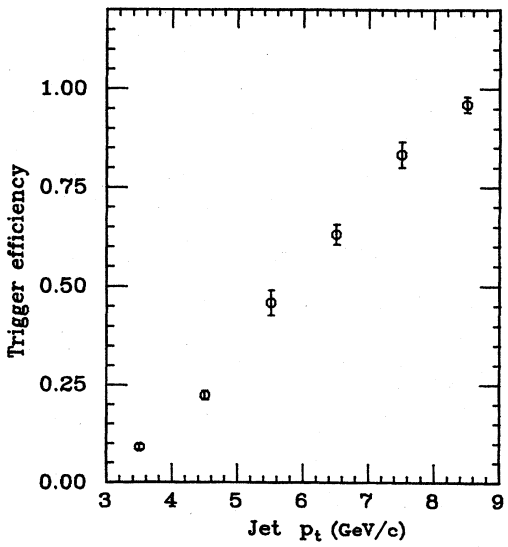

FIG. 10. The efficiency of the two-high trigger as a function of jet p_T, calculated from the Monte Carlo program.

Our fiducial volume of 60° to 100° yields $\Delta y_1 = \Delta y_2 = 0.73$. We assume that y_1 and y_2 are not dynamically correlated over this range.

The correction for events not originating in the target hydrogen was evaluated from the production vertex obtained using the charged-particle tracking-chamber data. The tracking was done for a subsample of the data (about

TABLE IV. The effect of varying assumptions on the size of the transverse shower spreading in the calorimeter on the calculated trigger efficiency. The two columns give as a function of p_T the ratio of the efficiency calculated for the largest reasonable deviation (smaller or larger) from the nominal spreading to the efficiency calculated using the nominal spreading.

Jet p_T (GeV/c)	Smaller spreading	Larger spreading
3—4	1.12	0.81
4—5	1.03	0.87
5—6	1.04	0.78
6—7	1.09	0.90

TABLE V. Ratio of trigger efficiency calculated (using the particles from the high-p_T jets only) using the ISAJET Monte Carlo to that calculated using the Monte Carlo described in the text.

p_T (GeV/c)	Trigger efficiency: ISAJET/E-609
3–4	0.65
4–5	0.67
5–6	0.78
6–7	0.95

40% of the total) and the nonhydrogen correction thus determined applied to the entire data sample. The correction was found to be independent of jet p_T and results in multiplying the observed number of events by a factor of (0.74 ± 0.10).

The number of events is the total number found corrected for nonjet background. As mentioned above we use the nonjet background from method II as given in Table III.

The resulting cross sections are given in Table VI. We list the value, its statistical error, and separate upper and lower systematic errors. The latter include an estimate of the error in the nonjet background correction added linearly to the systematic errors in the trigger efficiency discussed in Sec. III E. As mentioned above, we regard the 3.5-GeV/c point as having a large systematic uncertainty which is indicated in its systematic error.

These results are plotted in Fig. 11. The data points roughly follow an exponential in p_T. A fit to the form $A\exp(-Bp_T)$ yields

$$A=(2.2\pm0.6)\times10^{-28}\ \text{cm}^2/(\text{GeV}/c)^2$$

and

$$B=1.71\pm0.05\ (\text{GeV}/c)^{-1}\ .$$

If the 3.5-GeV/c point is excluded from the fit (its trigger efficiency and background contribution are the worst known of any of the points), there is very little change in the slope, B becomes $1.74\pm0.06\ (\text{GeV}/c)^{-1}$, while the intercept A becomes $(2.7\pm1.0)\times10^{-28}\ \text{cm}^2/(\text{GeV}/c)^2$.

It is important to note that these dijet cross sections can be regarded as essentially empirical; that is, they are the cross sections for an experimental solid angle of 2.7 sr per jet. Only the trigger efficiencies in Fig. 10 have a direct "theoretical" source, and they appear not to be very model dependent.

TABLE VI. The invariant cross section $d\sigma/dp_T{}^2dy_1dy_2$ at $y_1=y_2=0.18$ (80° c.m.) as a function of p_T measured in this experiment, including error estimates as described in the text.

Jet p_T (GeV/c)	Invariant cross section [cm^2/(GeV/c^2)]
3.5	$(4.9\pm0.8^{+2.7}_{-0.6})\times10^{-31}$
4.5	$(1.0\pm0.1^{+0.5}_{-0.1})\times10^{-31}$
5.5	$(1.7\pm0.5^{+0.8}_{-0.1})\times10^{-32}$
6.5	$(3.6\pm0.3^{+0.5}_{-0.2})\times10^{-33}$
7.5	$(4.6\pm0.8^{+0.7}_{-0.2})\times10^{-34}$
8.5	$(6.8\pm2.8^{+1.0}_{-0.3})\times10^{-35}$

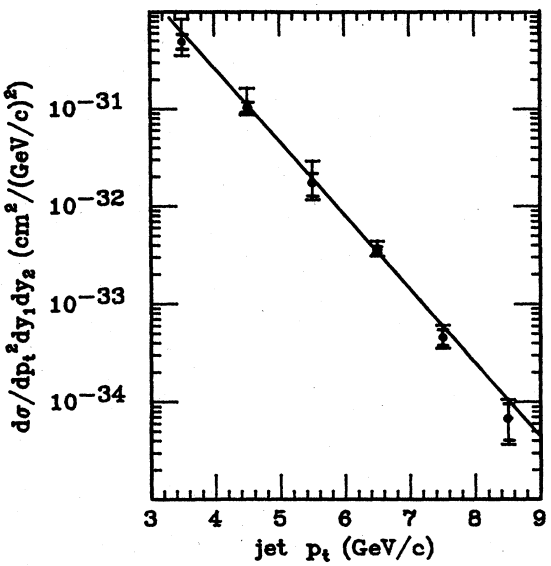

FIG. 11. The invariant cross section for dijet production versus p_T. The inner error bars are statistical and the outer error bars include systematic errors as described in the text. The line is a fit to the form $\exp(-Bp_T)$.

B. Comparison with theory

Figure 12 shows the data points again along with some theoretical calculations. The theoretical cross section for any given parton-parton scattering is given by[16]

$$d\sigma/dp_T{}^2dy_1dy_2=(\hbar c)^2(\hat{s}/s)\alpha_s{}^2F(x_1)F(x_2)d\sigma(\hat{s},\hat{t},\hat{u})/d\hat{t}\ .$$

The cross section is a function of three variables, p_T, y_1, and y_2, which determine x_1, x_2, and $\hat{t}$. We have calculated the cross section for $y_1=y_2=0.18$, corresponding to a θ of 80° in the c.m., summing over parton types in the proton, including u,d,s quarks and their antiquarks and gluons. The F's are the structure functions of the protons. One must choose the form of Q^2, which along with the QCD scale factor Λ determines the value of α_s and the magnitude of scale breaking in the structure functions. We have used the form for Q^2 recommended by Combridge, Kripfganz, and Ranft:[16] $Q^2=(\hat{s}\hat{t}\hat{u})^{1/3}$. We have also tried other forms of Q^2 and find little difference. The first-order QCD cross sections $d\sigma/d\hat{t}$ are well known.

The theoretical result depends on the structure functions used, especially on the gluon structure function, which is by far the least well known. The curves in Fig. 12 show several choices of the structure functions. The solid curve uses the determination of the structure functions by Gluck, Hoffman, and Reya.[17] Two simpler forms of the gluon structure function determined by Owens and Reya[18] are also shown, the "counting-rule"

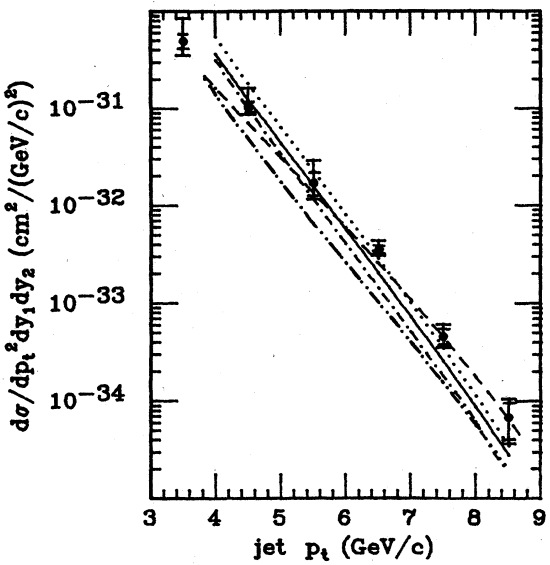

FIG. 12. Comparison of the measured dijet cross section (same points as Fig. 11) with theoretical predictions. The theoretical curves are based on various forms of the proton structure functions. The solid curve is based on Ref. 17. The dotted curve uses the counting-rule form of the gluon structure function, and the dashed curve the dynamical QCD form, both from Ref. 18. The dot-dashed curve and the dot-dot-dashed curve are based on the two sets of structure functions given in Ref. 19.

form as the dotted curve and the "dynamical QCD" form as the dashed curve. In all three curves the quark structure functions of Ref. 17 are used. All three curves use $\Lambda=0.4$ GeV/c. Also shown are the cross sections calculated using two sets of structure functions determined by Duke and Owens.[19] These two sets correspond to two different input assumptions about the gluon structure function at low Q^2. In their fits Duke and Owens allowed the value of Λ to vary. Their set 1, which yields the cross section shown by the dot-dashed curve, assumes a gluon structure function proportional to $(1-x)^6$ and finds $\Lambda=0.2$ GeV/c. Their set 2, which gives the dot-dot-dashed curve in Fig. 12, is proportional to $(1-x)^4$ and has $\Lambda=0.4$ GeV/c.

The agreement between experiment and theory is quite good, given the uncertainties in both experiment and theory. For instance, it is not known what the effects of higher-order diagrams are in the theory. The agreement in slope is probably the most significant feature, since the magnitude of the measured cross section is strongly dependent on the p_T scale which is known in the experiment only to about 7%. It should be relatively straightforward to compare our results with predictions of more refined theoretical models. Such models are normally evaluated using Monte Carlo programs; the experimental information contained in this paper should be sufficient to allow theoretical Monte Carlo predictions for comparison with our cross section results shown in Fig. 11.

There are several published results on single-jet cross sections.[4] Results on dijet cross sections (although not directly given as the invariant cross section as a function of p_T) have recently been published for $p\bar{p}$ collisions at $\sqrt{s}=540$ GeV from experiments at the CERN collider.[20]

V. SUMMARY

We have measured the invariant cross section for the production of jet pairs in 400-GeV/c pp collisions in the p_T range 4 to 9 GeV/c for each jet, over which the cross section varies by several orders of magnitude. In order to make this measurement, techniques for measuring jets and for estimating the background from nonjet events have been developed. Comparison of the results with theoretical calculations using proton structure functions and first-order QCD shows strikingly good agreement. The final result, with a 7% uncertainty in the p_T scale, can be represented by

$$d\sigma/dp_T^2 dy_1 dy_2=[(2.7\pm1.0)\times10^{-28}\ \text{cm}^2/(\text{GeV}/c)^2]\exp\{[-1.74\pm0.06\ (\text{GeV}/c)^{-1}]p_T\}$$

for p_T from 4 to 9 GeV/c.

ACKNOWLEDGMENTS

We would like to thank the many people at Fermilab and at the various institutions of this collaboration whose efforts made this experiment possible. This work was supported in part by the U. S. Department of Energy.

APPENDIX A: RESOLUTION EFFECTS

The invariant differential cross section

$$I(p_T)=d\sigma/dp_T^2 dy_1 dy_2$$

is a rapidly decreasing function of p_T. In the p_T range of this experiment $I(p_t)$ falls by a factor of 6 per GeV/c increase of p_T. (The counting rate dN/dp_T, including the two-high trigger requirement, falls by a factor of about 3 to 5 per GeV/c). A direct consequence of this rapid falloff is an extreme sensitivity of the measured cross section to the overall effective resolution function for the p_T of the jet.

The main resolution effects which we have taken into account in our analysis (and the approximate rms dispersion in p_T associated with each) are the following, in order of generally increasing complexity: (1) Random p_T

fluctuations due to calibration inaccuracies (4%), (2) finite angular resolution of the calorimeter towers (5%), (3) resolution width of the calorimeter response due to sampling fluctuations and to fluctuations in the $\pi^{\pm}/\pi^0$ energy partition in the hadronic showers (12%), and (4) the net effect of gain of nonjet particles and loss of jet fragments into and out of the cone used to find the jet (16%). Aside from these effects, there is also an overall 7% systematic uncertainty in the p_T scale.

Effect 4 is a delicate model-dependent effect, involving jet fragmentation functions, the contributions of nonjet particles, and subtle issues regarding separation of real jets from background fluctuations. Since this resolution effect is larger than those involving the energy resolution of the apparatus, it is the main factor which needs to be taken into account in comparing predictions of theoretical models with our experimental results. We discuss these issues further in Appendix B.

We have evaluated the above resolution effects by making detailed Monte Carlo simulations which use the measured energy response functions of the calorimeter. We have also explored the sensitivity of this procedure to uncertainties in the Monte Carlo model and in the measured response functions.

One critical conclusion is already documented in previous papers.[9] A tail of the apparatus resolution function which extends toward large values of (apparent) p_T can lead to huge shifts in the apparent cross section. Our calorimeter was designed to avoid such a tail, and its measured resolution function is satisfactory for use with the observed steeply falling p_T spectrum.

An illustrative but much oversimplified formula for the change in cross section due to a dispersion in resolution σ is

$$f_{\text{obs}}(p_T)=f_{\text{true}}(p_T)+0.5(d^2f/dp_T{}^2)\sigma^2+\cdots$$

or

$$\Delta f=0.5f''\sigma^2 .$$

This formula assumes that the effective resolution function is symmetric and unbiased with an rms width of σ. If we take σ^2 to be the sum of squares of individual dispersions enumerated in the above list, we have at $p_T=6$ GeV/c, $\sigma=1.3$ GeV/c and $f_{\text{obs}}=2.7f_{\text{true}}$.

This increase in the apparent cross section can be corrected for by making an 8% downward shift in the p_T scale. As described in Sec. II, we have chosen to correct the experimental p_T scale rather than the measured cross section, using a correction based on a detailed Monte Carlo evaluation of the resolution effects.

APPENDIX B: EVALUATION OF JET BACKGROUND

At the simplest level, it is necessary to distinguish true jet structure from fluctuations which will occur in nonjet multiparticle final states. More generally, it is necessary to determine the effect of defining a jet cone which includes some nonjet (background) particles, and which is not generally large enough to contain all of the jet fragmentation particles. This determination becomes increasingly difficult as the jet p_T decreases and as the ratio of jet p_T to total final-state E_T decreases.

We have used two different kinds of approaches to background evaluation. The first approach is based on model-independent methods, of which we considered two.

The first model-independent method involves randomizing the directions of final-state particles. This is done subject to the constraint that the vector sum of p_T for all particles detected in the calorimeter is preserved after the randomization. Of course the magnitude of p_T of each particle and thus the total E_T are also invariant under this randomization. The overall effect is to generate a new ensemble of events whose outgoing observed particles have the minimum angular correlations which are consistent with momentum conservation (and of course with the actual p_T distribution of particles within individual events).

The second model-independent method is to use the observed single-particle distributions in p_T and $\theta_{\text{c.m.}}$ for global E_T trigger events in the appropriate E_T range to generate artificial multiparticle events which are random except for having detected particles that satisfy momentum conservation to the same degree as do the real events.

It is important to note that the presence of real jets in the data will lead to an overall single-particle p_T distribution which is "harder" than otherwise, as well as to positive correlations between high values of p_T for two or more particles within an individual event. Randomizing the particle directions removes neither of these jet effects. The second method removes p_T correlations between particles in an event, but does not remove the hard-p_T spectrum. Thus the background estimated by the above methods is an upper limit to the actual nonjet background, with the limit expected to be lower (more stringent) for the second method.

The second kind of approach to background estimation requires the use of specific models of jet production. By analyzing Monte Carlo-generated events in the same way as actual events, and by then making the randomization tests for "nonjet background," it is possible to compare directly the amount of background in the data with that in the model.

We have made several such Monte Carlo evaluations of background and resolution, as described in the main part of the paper, and have reached two primary conclusions. First, when the jet cone half angle is chosen (55° c.m.) to yield the input cross section for Monte Carlo events, there is a dispersion of roughly 1 GeV/c (at $p_T=6$ GeV/c) in the observed jet momentum, due to fluctuations in jet fragmentation lost from and beam-jet particles gained by the cone. This is an unavoidable fluctuation which is a major component of the "experimental" resolution function. This fluctuation has a significant effect upon the cross section measured as described in Appendix A.

The second conclusion is that the background at a given p_T, as evaluated using the model-independent randomizing processes described above, arises from the much more frequent jets of lower p_T combining with fluctuations in beam jet fragmentation particles. However, this background from lower-p_T jets is not a true background, for its effects are already accounted for in the process of

correcting for the fluctuations described in the previous paragraph.

As described in the main part of the paper, we find that the real data and Monte Carlo events do behave very similarly under randomization. This result implies that the randomized background is in fact a conservative upper limit to the amount of real nonjet background, in agreement with the above expectation.

---

*Present address: Dept. of Physics, University of Arizona, Tucson, Arizona 85721.

†Present address: University of Science and Technology of China, Hefei, Anjui, Peoples Republic of China.

‡Present address: NRC Democritos, Athens, Greece.

§Present address: Charles Evans Associates, 1670 S. Amphlett Blvd., San Mateo, California 94402.

**Present address: Exxon Corporation, Houston, Texas.

††Present address: LeCroy Research Systems, 700 Main St., Spring Valley, New York 10977.

[1]Phys. Scr. **19**, 69 (1979), contains references to the earliest work.

[2]M. Banner *et al.*, Phys. Lett. **118B**, 203 (1982).

[3]G. Arnison *et al.*, Phys. Lett. **123B**, 115 (1983).

[4]T. Akesson *et al.*, Phys. Lett. **123B**, 133 (1983); **118B**, 185 (1982); **118B**, 193 (1982).

[5]C. DeMarzo *et al.*, Phys. Lett. **112B**, 173 (1982); Nucl. Phys. **B211**, 375 (1983); **B234**, 1 (1984).

[6]B. C. Brown *et al.*, Phys. Rev. D **29**, 1895 (1984).

[7]W. Selove, in *Proceedings of the 21st International Conference on High Energy Physics, Paris, 1982,* edited by P. Petiau and M. Porneuf [J. Phys. (Paris) Colloq. **43**, C3-131 (1982)]; M. W. Arenton *et al.*, Phys. Rev. Lett. **53**, 1988 (1984).

[8]L. Cormell *et al.*, IEEE Trans. Nucl. Sci. **NS-29**, 307 (1982); K. A. Johns, Master's thesis, Rice University, 1983.

[9]M. Dris, Nucl. Instrum. Methods **161**, 311 (1979); W. Selove *et al.*, University of Pennsylvania Report No. UPR-75E, 1980 (unpublished).

[10]K. S. Nelson and A. R. Erwin, IEEE Trans. Nucl. Sci. NS-30, 146 (1983).

[11]R. Singer, T. Fields, and W. Selove, Phys. Rev. D **25**, 2451 (1982).

[12]M. D. Corcoran (unpublished).

[13]R. D. Field and R. P. Feynman, Nucl. Phys. **B136**, 1 (1978).

[14]R. K. Bock *et al.*, Nucl. Instrum. Methods **186**, 533 (1981).

[15]F. E. Paige and S. D. Protopopescu, in *Proceedings of the 1982 DPF Summer Study on Elementary Particle Physics and Future Facilities, Snowmass, Colorado,* edited by R. Donaldson, R. Gustafson, and F. Paige (Fermilab, Batavia, Illinois, 1982), p. 471.

[16]B. L. Combridge, J. Kripfganz, and J. Ranft, Phys. Lett. **70B**, 234 (1977).

[17]M. Gluck, E. Hoffmann, and E. Reya, Z. Phys. C **13**, 119 (1982).

[18]J. F. Owens and E. Reya, Phys. Rev. D **17**, 3003 (1978).

[19]D. W. Duke and J. F. Owens, Phys. Rev. D **30**, 49 (1984).

[20]G. Arnison *et al.*, Phys. Lett. **136B**, 294 (1984); P. Bagnaia *et al.*, *ibid.* **138B**, 430 (1984).